DETERMINING RUBIDIUM NUMBER DENSITY BY MEASURING FARADAY ROTATION NEAR RESONANCE

Emmanuel Soon Yi En[1], Kendrick Wong Wei Xiang[2], Hillson Hung Fong Bok[2]
[1]Anglo-Chinese School (Independent), 121 Dover Rd, Singapore 139650
[2]DSO National Laboratories, 12 Science Park Dr, Singapore 118225

1 Abstract

Rubidium number density is a critical parameter in quantum technologies such as atomic clocks, magnetometers, and super-radiance systems. This study introduces a novel approach leveraging Faraday Rotation to accurately determine rubidium vapour density by targeting D2 transition frequencies close to resonance near 780 nm. We employ balanced polarimetry with a bias field of 0.1 T without relying on extreme magnetic fields (0.8–1T), achieving a maximum rotation angle of 0.0175 radians. This is achieved by targeting frequencies close to resonance with a small laser detuning. Despite facing challenges such as magnetic field stability and potential Zeeman effect interference, our method offers a practical solution for rubidium vapour characterization.

2 Introduction

Determining the precise numerical density of rubidium vapor is of importance in the field of quantum physics. Atomic density is crucial for calculating phenomena in quantum optics, such as spin-exchange optical pumping, which is responsible for sensitive magnetometers. [1] Additionally, atomic number density is significant in building quantum sensing systems that require high degrees of precision, such as atomic clocks and super-radiance. [2] In a pure sample, the number density of rubidium is purely dependent on temperature, whereby formulas such as Killian's empirical formula are employed to give an estimate of rubidium-85 or rubidium-87 density. [3] However, there is currently no purpose-built laboratory equipment to characterise these rubidium cells. Various attempts have been made to remotely sense rubidium densities, ranging from optical absorption, combined fluorescence and absorption measurements. [4] These experiments have significant errors due to depopulation of the energy level, self-absorption, the effects of the glass cell, and power loss. In this paper, we measure Faraday Rotation from an external magnetic field to determine rubidium number density, modifying a method by Shang et al, with smaller laser detuning and lower magnetic fields. [5]

3 Theory

3.1 Faraday Rotation

Faraday Rotation is a phenomenon whereby a linearly polarised beam passing a polarisable gaseous medium placed in a uniform and static magnetic field experiences a rotation in its polarisation angle relative to the incident wave. [6] This is mathematically expressed as $\theta_B(\lambda) = V(\lambda)Bl$, whereby $\theta_B(\lambda)$ rotation angle, B is the magnetic field strength, l is the path length, and V is the Verdet constant, a unique material property. [7] Our method utilises a balanced photodetector to precisely measure the angle of rotation. Since Faraday Rotation alters the ratio of right- to left-circularly polarised light [8] from an initial 1:1 ratio, the deviation in this ratio when a magnetic field is applied corresponds directly to the extent of rotation, providing a sensitive means [9] to deduce the medium's density.

3.2 The Lorentz Model

Using the Lorentz model, we model the atom as a damped harmonic oscillator. [10] The electron is the oscillator bound to the nucleus by a harmonic force. The "dampening" of the oscillator arises from spontaneous emission, whereby the electron reverts back to a lower energy level without external stimulus. This equation of motion is expressed mathematically as:

$$m\ddot{x} + m\gamma\dot{x} + m{\omega_0}^2 x = -qE_0 e^{-i\omega t} \tag{1}$$

Where the term $m\ddot{x}$ represents the inertia of an electron due to acceleration under a force, $m\gamma\dot{x}$ the resistive forces damping the electron's oscillation, and $m{\omega_0}^2 x$ the periodic oscillating force acting on the electron by the atom. Lastly, $-qE_0 e^{-i\omega t}$ is the total driving force exerted by an oscillating electric field, a component of light, an electromagnetic wave, on the electron. We add a term to the Lorentz model to account for the force introduced by a magnetic field. The sign depends on the oscillation direction of the electron. [11]

$$F_B = \mp q\omega B x \tag{2}$$

3.3 Derivation of Faraday Rotation Angle

The combined equation of motion is given by

$$m\ddot{x} + m\gamma\dot{x} + m{\omega_0}^2 x \mp q\omega B x = -qE_0 e^{-i\omega t} \tag{3}$$

We assume the solution has the form:

$$x(t) = x_o e^{-i\omega t}$$

Where x_o is given by

$$x_0 = \frac{\frac{qE_0}{m}}{\omega^2 - {\omega_0}^2 \mp \frac{qB}{m}\omega + i\gamma\omega} \tag{4}$$

Since electron displacement is related to dipole moment and polarizability:

$$d = -cx = \alpha(\omega)E \tag{5}$$

Thus, polarizability is given by:

$$\alpha(\omega) = \frac{\frac{q^2}{m}}{{\omega_0}^2 \pm \frac{qB}{m}\omega - \omega^2 - i\gamma\omega} \tag{6}$$

We divide polarisation by the electric field E to give the susceptibility:

$$X(\omega) = \frac{\frac{Nq^2}{m\epsilon_0}}{{\omega_0}^2 \pm \frac{qB}{m}\omega - \omega^2 - i\gamma\omega} \tag{7}$$

We derive the refractive index by extracting the real component, the phase index from (7)

$$n_{\pm} = 1 + \left(\frac{Nq^2}{2m\epsilon_0}\right)\left(\frac{{\omega_0}^2 - \omega^2 \mp \omega_B\omega}{({\omega_0}^2 - \omega^2 \mp \omega_B\omega)^2 + \gamma^2\omega^2}\right) \tag{8}$$

Then, the change in rotation angle of the optical axis, weighed by polarisation strength and abundance, is

$$\Delta\Phi = \frac{(n_+ - n_-)\omega L}{2c} \tag{9}$$

3.4 Absorption Spectroscopy

From the Lorentz model, when the frequency of light, an electromagnetic wave with an electrical component, matches the natural resonance frequency, ω_0, of the atomic transition, the driving force remains constant, but the energy transfer from the photon is maximum. When the energy possessed by the photon, (which is dependent on frequency in $E = hv$), matches the energy required to undergo an atomic transition, the electron undergoes that transition. The absorption of a photon results in a net loss of intensity as light transmits through the medium. In absorption spectroscopy, a photodetector is used to identify frequencies where dips or "peaks" in transmission occur. By sweeping the laser across a range of frequencies, we can precisely target and study various atomic transitions, each corresponding to specific transition frequencies.

3.4.1 Transition States – Energy Levels

Atoms have discrete energy levels that electrons can occupy. When electrons transition between these energy levels due to excitation by a specific frequency of light, they give rise to different transition lines, denoted by the quantum number F. The allowed transitions follow the selection rules, where $F^1 = F \pm 1$ or F. The theoretical data for the Rb spectral lines has been calculated and documented by Steck [12,13]. Referring to Figure 1, the D2 line of Rb-87 occurs at a frequency of approximately 384 THz and baseline wavelength of 780 nm.

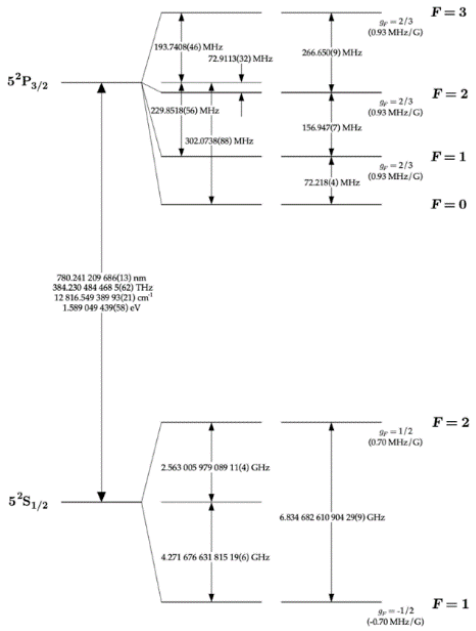

Figure 1: Steck's Calculation of the D2 Transitions

3.4.2 Transition States – Hyperfine Splitting

The left section of Figure 1 details the hyperfine splitting of the energy levels. Hyperfine splitting occurs due to the interaction between the nuclear spin and the magnetic field generated by the electrons. This field arises from both the orbital motion of the electrons and their spin angular momentum, causing energy levels to split into sub-levels. There are six main transitions for Rb-85 and Rb-87, each exerting unique effects on Faraday Rotation due to our proximity to resonance. Unlike the Shang et al. paper, which treated the entire D1 line as a single entity and operated with far detuning from resonance, we calculate a weighted oscillator strength for each transition and solve our equation accordingly.

3.5 Determining Faraday Rotation of Hyperfine Transitions

For each hyperfine transition, the polarization rotation against frequency is given by

$$\Delta\varphi = \Delta\Phi f_{ge}\kappa \tag{10}$$

Whereby f_{ge} is the oscillator strength and κ is a weight described by Happer [14]. Happer's analysis only considers the fine structure and works in the J basis. To determine the weights of the hyperfine transitions, we utilize his technique to derive κ in the F basis as follows.

$$\kappa = \frac{g_{f_g}\left(2 + F_g(F_g+1) - F_e(F_e+1)\right)}{4} + \frac{g_{f_e}\left(2 + F_e(F_e+1) - F_g(F_g+1)\right)}{4} \tag{11}$$

4 Materials and Methods

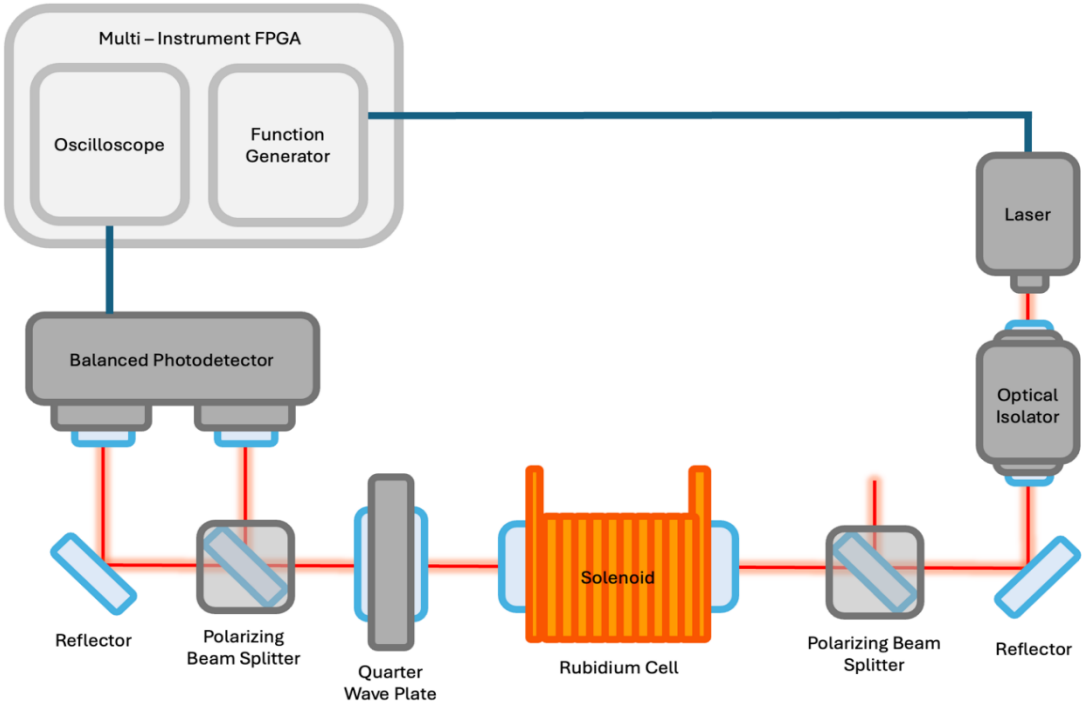

Figure 2: Experimental Setup Diagram

The function generator produced a 100 Hz sawtooth signal with a 3.000 V peak-to-peak amplitude to sweep the laser's frequency, with voltage-induced thermal expansion of the cavity (between the half and full mirrors) increasing the wavelength and allowing for a 10GHz range centred at the Rubidium 87 F2-F3 transition. The setup is mounted on an optical table to isolate it from external noise. This light is directed into an adjustable polarizing beam splitter, which controls the laser's power and ensures that the incident beam is horizontally polarised [15].

A 3D-printed holder enclosed the rubidium cell, around which 800 coils of copper wire were wound to form an 8 cm solenoid. Current was varied through values of 0, 400, 500, 600, 710, and 810 mA. When light passes through the rubidium cell, the magnetic field of the solenoid induces Faraday rotation. This alters the proportions of left and right circularly polarized light, rotating the plane of linear polarization by a specific angle. The rotated light then passes through a quarter-wave plate, converting circularly polarized light back into linearly polarized light. The quarter-wave plate also calibrates the initial proportion of detected linearly polarized light [16].

Finally, the polarizing beam splitter separates the horizontally and vertically polarized light, directing them into Channels A and B of the photodetector for measurement. Without Faraday rotation, the polarization state remains unchanged, and no significant intensity difference between Channels A and B would be observed, except near resonance frequencies.

5 Results

The change in the polarisation angle is thus given by the equation

$$\Delta\theta = \tan^{-1}\left(\frac{H}{V}\right) \tag{12}$$

Where H is horizontally polarized light coming from Channel A and V is vertically polarized light coming from Channel B. As frequency increases, the fit of our experimental to our theory values becomes more congruent, and the final theoretical graph was obtained by adjusting the rubidium density to obtain the best theoretical and experimental fit.

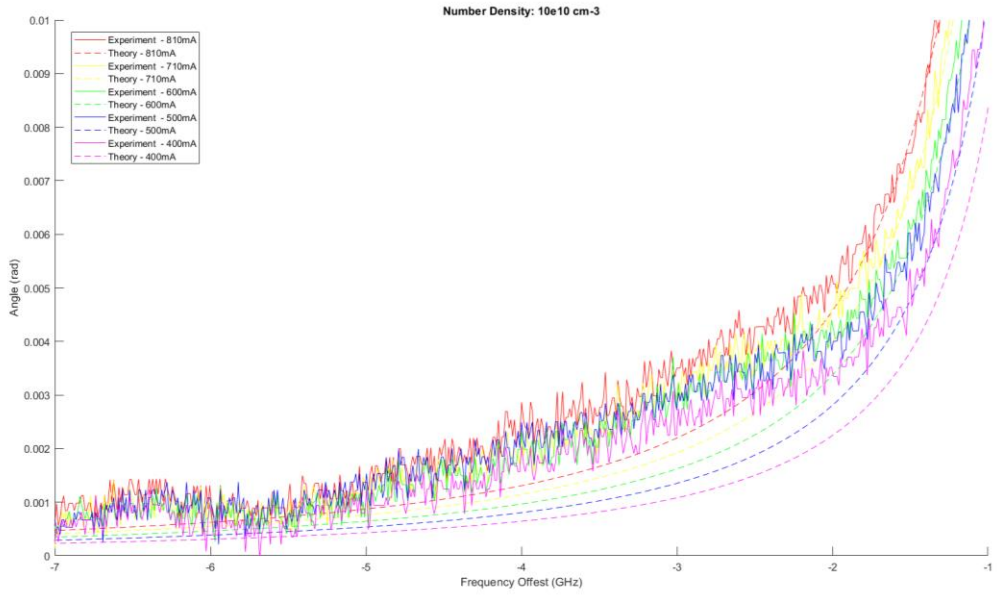

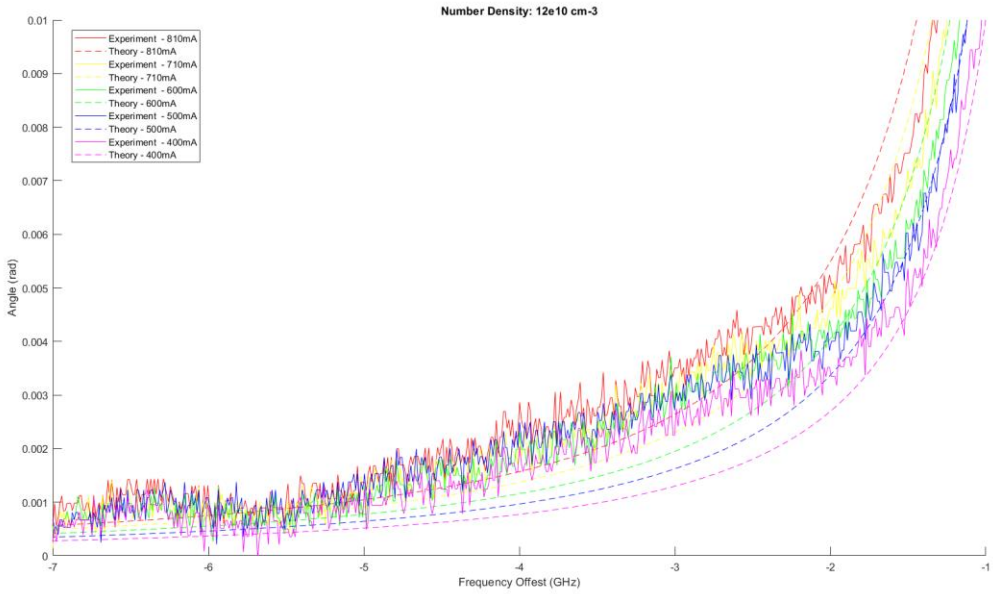

Figure 3: Graphs of Rotation Angle against Frequency Offset

6 Discussion

Our experiment's calculated Rubidium density was in a range of $10x10^{10} – 12x10^{10}$ atoms/cm^3, which differs from the empirical formula of Killians by one order of magnitude higher. This is

expected and congruent with experimental results from Shang [5], who experienced about a ¼ magnitude deviation, and Speck [4], who garnered a low 4% accuracy. While we are still unable to verify this experimental module for high precision, we are satisfied that the rough order of magnitude is congruent, and this method holds fast, but needs further refinement.

6.1 Advantages

Our experiment demonstrates an advantage over a similar study by Shang et al., as we can target wavelengths closer to resonance to observe larger rotation angles. [17] We achieved a maximum rotation angle of 0.0175 radians - one order of magnitude higher than the 0.0035 radians observed in Shang et al. This improvement eliminates the need for complex or hard-to-access equipment, such as a strong permanent magnet with a field exceeding 800 Gauss or a Faraday modulator to detect minute Faraday rotation angles. Using simpler and more accessible equipment, our setup remains simple and practical.

In typical setups, the inconsistent effects of laser transmission through the glass and weak internal reflections lead to unreliable results. One could attempt to compensate for these losses by scaling the signal intensity, but this approach makes large assumptions. Our method, uses ratio analysis of two spectral channels, which inherently accounts for intensity losses through the glass and air medium. While it is true that polarization-dependent losses at the glass surface could potentially affect signal integrity, the ratio analysis normalizes the variations introduced by polarization-dependent transmission, as both spectral channels traverse the same optical path and experience similar polarization effects.

6.2 Limitations

It was important to note that two magneto-optical effects, the Zeeman and the Faraday effect, both affect the polarisation of the light and thus the final calculation. While we detuned the laser by adjusting the calibration setpoint to cover a frequency range sufficiently far away from the Zeeman effect, there was a possibility of interference between the two magneto-optical effects, with difficulty distinguishing Faraday rotation signals from Zeeman-related distortions.

7 Conclusion

This study introduces a practical method for determining rubidium vapor density using Faraday Rotation with balanced polarimetry. The approach achieves higher rotation angles of up to 0.0175 near resonance frequencies of the D2 line while minimizing errors from glass transmission and polarization-dependent losses, but also encounters an additional source of error from the Zeeman effect due to small detuning.

8 Acknowledgements

I would like to express my heartfelt gratitude to my DSO mentors, Kendrick and Hillson, for their unwavering support throughout my internship. I am truly thankful for their guidance and for the opportunity to learn from their expertise.

9 References

[1] J. Rantaharju, M. Hanni, and J. Vaara, “Polarization transfer in a spin-exchange optical-pumping experiment,” Physical Review. A/Physical Review, A **102**(3), (2020).

[2] J. Vanier, “Atomic clocks based on coherent population trapping: a review,” Applied Physics B **81**(4), 421–442 (2005).

[3] “Vapor Reference Cells,” (n.d.).

[4] A.M. Van Der Spek, J.J.L. Mulders, and L.W.G. Steenhuysen, “Vapor pressure of rubidium between 250 and 298 K determined by combined fluorescence and absorption measurements,” Journal of the Optical Society of America B **5**(7), 1478 (1988).

[5] H. Shang, B. Zhou, W. Quan, H. Chi, J. Fang, and S. Zou, “Measurement of rubidium vapor number density based on Faraday modulator,” Journal of Physics D Applied Physics **55**(33), 335106 (2022).

[6] P. Fumagalli, and J. Schoenes, *Magneto-Optics: An Introduction* (Walter de Gruyter GmbH & Co KG, 2021).

[7] *Semiconductors and Semimetals* (Academic Press, 1967).

[8] K. Ferrière, J.L. West, and T.R. Jaffe, “The correct sense of Faraday rotation,” Monthly Notices of the Royal Astronomical Society **507**(4), 4968–4982 (2021).

[9] G. Litfin, C.R. Pollock, R.F. Curl, and F.K. Tittel, “Sensitivity enhancement of laser absorption spectroscopy by magnetic rotation effect,” The Journal of Chemical Physics **72**(12), 6602–6605 (1980).

[10] A.M. Perelomov, and V.S. Popov, “The Lorentz Group as a Dynamic Symmetry Group of the Hydrogen Atom ” Journal of Experimental and Theoretical Physics **23**, 118 (1966).

[11] K.E. Oughstun, and R.A. Albanese, “Magnetic field contribution to the Lorentz model,” Journal of the Optical Society of America A **23**(7), 1751 (2006).

[12] Daniel A. Steck, ‘‘Rubidium 85 D Line Data,’’ available online at http://steck.us/alkalidata (revision 2.3.3, 28 May 2024).

[13] Daniel A. Steck, ‘‘Rubidium 87 D Line Data,’’ available online at http://steck.us/alkalidata (revision 2.3.3, 28 May 2024).

[14] W. Happer, and B.S. Mathur, “Effective Operator Formalism in Optical Pumping,” Physical Review **163**(1), 12–25 (1967).

[15] M. Jeannin, E. Cosentino, S. Pirotta, M. Malerba, G. Biasiol, J.-M. Manceau, and R. Colombelli, “Low-intensity saturation of an ISB transition by a mid-IR quantum cascade laser,” Applied Physics Letters **122**(24), (2023).

[16] Z. Chen, Y. Gong, H. Dong, T. Notake, and H. Minamide, “Terahertz achromatic quarter wave plate: Design, fabrication, and characterization,” Optics Communications **311**, 1–5 (2013).

[17] P.S. Hsu, A.K. Patnaik, and G.R. Welch, “Nonlinear magneto-optic polarization rotation with intense laser fields,” Physical Review A **78**(5), (2008).

10 Appendix

10.1 Equipment

Equipment	Precision	Quantity
Moku Oscilloscope Go	500 KSa/s	1
PDB210A/M - Free-Space Balanced Photodetector	2.2 pW/√Hz	1

Software	Purpose
Google Collab	Coding & Data Cleaning
Koheron	Laser Control
Moku Software	Oscilloscope & Function Generator

Additional Equipment	Quantity
GC25075-RB - Rubidium Borosilicate Reference Cell	1
Mirror	2
Polarising Beam splitter	2
740 nm laser	1
Variable power output	1
Optical Isolator	1
Quarter Wave Plate	1
Custom 3D printed holder	1
3 mm copper wire	1
Vibration Cancelling Optical Table	1

10.2 Images

Figure 4: Moku Oscilloscope Go

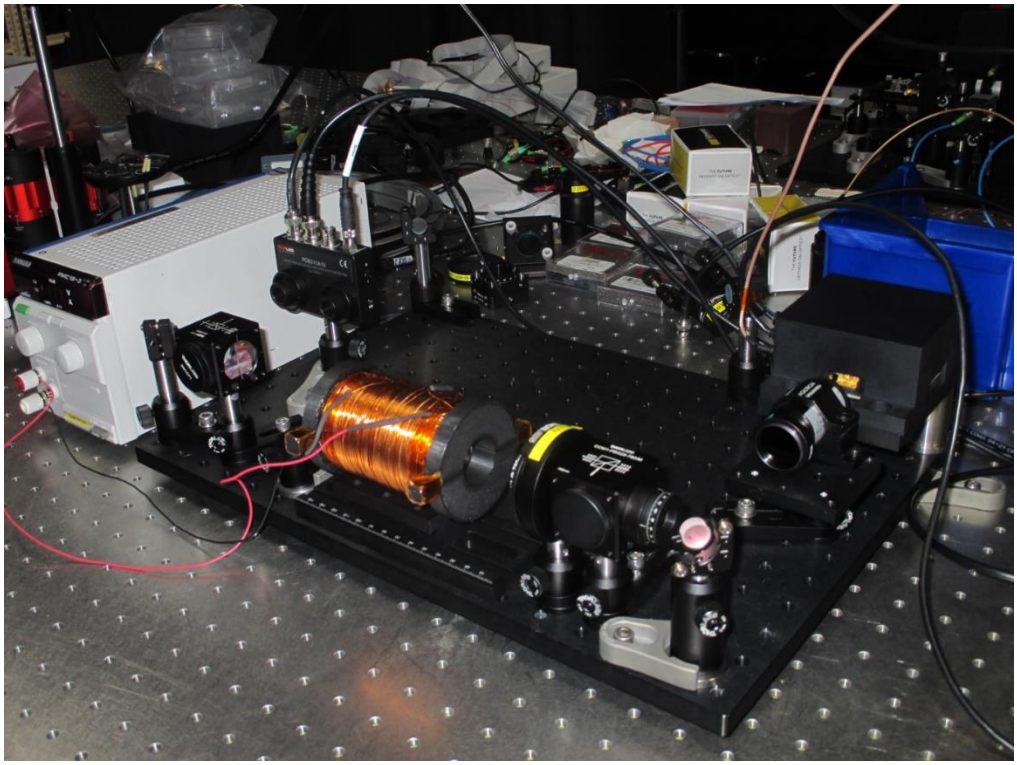

Figure 5: Image of experimental diagram